J|A|C|S
ARTICLES

Published on Web 06/01/2009

Luminescent Cyclometalated *N*-Heterocyclic Carbene-Containing Organogold(III) Complexes: Synthesis, Characterization, Electrochemistry, and Photophysical Studies

Vonika Ka-Man Au, Keith Man-Chung Wong, Nianyong Zhu, and Vivian Wing-Wah Yam*

Centre for Carbon-Rich Molecular and Nano-Scale Metal-Based Materials Research and Department of Chemistry, The University of Hong Kong, Pokfulam Road, Hong Kong

Received April 7, 2009; E-mail: wwyam@hku.hk

Abstract: A new class of luminescent mononuclear and dinuclear *N*-heterocyclic carbene-containing gold(III) complexes has been synthesized and characterized. The X-ray crystal structures of most of the complexes have also been determined. Electrochemical studies reveal a ligand-centered reduction originated from the RC^N^CR moieties with no oxidation waves. Interestingly, one of the dinuclear complexes exhibited two distinct reduction couples instead of one with the first reduction occurring at less cathodic potential, probably related to the splitting of the π^* orbital-based LUMO resulting from intramolecular $\pi-\pi$ interaction. The electronic absorption and luminescence behaviors of the complexes have also been investigated. In dichloromethane solution at room temperature, the low-energy absorption bands are assigned as the intraligand $\pi-\pi^*$ transition, with mixing of a charge transfer character from the aryl ring to the pyridine moiety of the cyclometalating RC^N^CR ligand. The low-energy emission bands are ascribed to origins mainly derived from the intraligand $\pi-\pi^*$ states with an aryl to pyridine charge transfer character of the cyclometalating RC^N^CR ligand.

Introduction

Traditionally carbenes have been considered to be unstable, short-lived, electron-deficient two-coordinate carbon compounds with two non-bonding electrons. However, the picture no longer held when Öfele[1] and Wanzlick[2] first reported the use of *N*-heterocyclic carbenes (NHCs) as ligands independently in 1968. In 1991, Arduengo and co-workers successfully isolated a free imidazole-2-ylidene,[3] which marks a new era in organometallic chemistry by providing access to a huge number of metal−carbene coordination complexes. NHCs, singlet carbenes incorporated in a nitrogen-containing heterocycle, are found to have strikingly similar properties as organophosphanes PR_3 in terms of their electronic properties and thus metal coordination chemistry according to a study by Herrmann and co-workers in the early 1990s.[4] In contrast to traditional electron-deficient carbenes, NHCs are found to be electron-rich and stable and can be isolated. The singlet NHCs are electronically stabilized by the interaction of the empty p-orbital with the two neighboring nitrogen lone pairs.[5] This unexpected stability of NHCs has offered an exciting area of research in organometallic chemistry, nurturing the development of numerous NHC-containing transition metal complexes.

Organometallic complexes incorporated with NHC moieties have been widely studied. Examples of metal centers include Ag(I),[6] Ru(II),[7] Pt(II),[8] Pd(II)[9] and Au(I).[10] In particular, much attention has been drawn toward NHC-containing Au(I) complexes despite the chemical inertness of metallic gold. A number of reports have been published on functional materials containing Au(I) NHC moieties, which possess applications in various fields. For instance, Lin and co-workers have prepared the first liquid crystalline Au(I) NHC complexes by making use of benzimidazolium salts with long alkyl side chains on the carbene nitrogen atoms.[11] In addition to a bilayer lamellar structure with Au···Au distances of ~3.6 Å, these Au(I) NHC complexes were found to have low transition temperatures, broad mesophase temperature ranges, and high thermal stabilities compared to other Au(I)-containing liquid crystals. On the other hand, Au(I) NHC complexes also have potential use in pharmaceuticals.

(1) Öfele, K. *J. Organomet. Chem.* **1968**, *12*, P42−P43.
(2) Wanzlick, H. W.; Schönherr, H. J. *Angew. Chem., Int. Ed.* **1968**, *7*, 141–142.
(3) Arduengo, A. J., III; Harlow, R. L.; Kline, M. A. *J. Am. Chem. Soc.* **1991**, *113*, 361–363.
(4) (a) Herrmann, W. A. *Angew. Chem., Int. Ed.* **2002**, *41*, 1290–1309. (b) Herrmann, W. A.; Mihalios, D.; Öfele, K.; Kiprof, P.; Belmedjahed, F. *Chem. Ber.* **1992**, *125*, 1795–1799. (c) Öfele, K.; Herrmann, W. A.; Mihalios, D.; Elison, M.; Herdtweck, E.; Scherer, W.; Mink, J. *J. Organomet. Chem.* **1993**, *459*, 177–184. (d) Herrmann, W. A.; Öfele, K.; Elison, M.; Kühn, F. E.; Roesky, P. W. *J. Organomet. Chem.* **1994**, *480*, C7−C9.
(5) Glorius, F. *Top. Organomet. Chem.* **2007**, *21*, 1–20.
(6) Lin, I. J. B.; Vasam, C. S. *Coord. Chem. Rev.* **2007**, *251*, 642–670.
(7) Weskamp, T.; Schattenmann, W. C.; Spiegler, M.; Hermann, W. A. *Angew. Chem., Int. Ed.* **1998**, *37*, 2490–2493.
(8) Ahrens, S.; Herdtweck, E.; Goutal, S.; Strassner, T. *Eur. J. Inorg. Chem.* **2006**, 1268–1274.
(9) Peris, E.; Loch, J. A.; Mata, J.; Crabtree, R. H. *Chem. Commun.* **2001**, 201–204.
(10) Lin, I. J. B.; Vasam, C. S. *Can. J. Chem.* **2005**, *83*, 812–825.
(11) Lee, K. M.; Lee, C. K.; Lin, I. J. B. *Angew. Chem., Int. Ed.* **1997**, *36*, 1850–1852.

10.1021/ja9027692 CCC: $40.75

Baker, Berners-Price, and co-workers have designed a class of dinuclear Au(I) NHC complexes with promising antimitochondrial activities.[12] The luminescent properties of these complexes allow cellular imaging by confocal fluorescence microscopy without the need of additional fluorescence tags. A series of photochromic diarylethene-containing NHCs and their Ag(I), Pd(II) and Au(I) complexes have also been reported very recently.[13]

Gold(III) complexes, in contrast to the gold(I) system with extensive reports on luminescence studies, were seldom found to be emissive, probably due to the presence of low-energy d-d ligand field (LF) states,[14] which would quench the luminescence excited state via thermal equilibrium or energy transfer.[15] In order to enhance the luminescence of gold(III) complexes, good σ-donating ligands have been introduced to render the gold(III) metal center more electron-rich and raise the energy of the d-d states. This concept was demonstrated by the reports on luminescent organogold(III) diimine complexes, $[AuR_2(L\text{^}L)]ClO_4$ (R = mes, CH_2SiMe_3, L^L = 2,2′-bpy, phen, dpphen)[16] and cyclometalated alkynylgold(III) complexes, [Au(RC^N(R′)^CR)(C≡CR″)].[17b−d]

Although a number of NHC-containing Au(I) complexes have been reported in the literature, related Au(III) complexes have rarely been communicated. Recently, Nolan and co-workers reported the synthesis of the complex $(NHC)Au^{III}Br_3$, which could catalyze the polymerization of styrene at room temperature in the presence of $NaBAr'_4$.[18] Later on, Huynh and co-workers have reported the preparation of the first Au(III) benzimidazolin-2-ylidene complex, *trans*-$[AuI_2(^iPr_2\text{-bimy})_2]BF_4$. The photophysical properties of the complex in the solid state at room temperature have been studied.[19] Both kinds of Au(III) NHC complexes reported by the groups of Nolan and Huynh were prepared by oxidative addition, in which bromine or iodine was allowed to react with the Au(I) NHC precursor complexes in dichloromethane solution at low to ambient temperature. Up to the present moment, there are only a few examples of Au(III) NHC complexes in the literature, and no reports on the direct incorporation of NHC ligands into the Au(III) metal center has ever been published. Hence, there is much room for the investigation of NHC-containing Au(III) complexes, especially in relation to their syntheses and photophysical properties.

In light of the strong σ-donating properties of NHC ligands, as well as limited reports on NHC-containing Au(III) complexes, a program was launched to investigate the incorporation of *N*-heterocyclic carbenes into organogold(III) systems, which we believe would render the gold(III) metal center less electrophilic and contribute to interesting luminescence properties. Herein, a series of mononuclear and dinuclear luminescent NHC-containing organogold(III) complexes with various cyclometalated and *N*-heterocyclic carbene ligands have been synthesized and characterized (Chart 1). In contrast to previously reported Au(III)-NHC complexes, which were synthesized through the oxidative addition reactions of their Au(I)-precursor complexes, the preparation of such NHC-containing cyclometalated Au(III) complexes involves the direct incorporation of NHC ligand into the Au(III) starting materials, [Au(RC^N^CR)Cl]. In addition to the synthetic methodology and characterization of the complexes, their electrochemical and photophysical behaviors have also been studied.

Results and Discussion

Synthesis and Characterization. The incorporation of *N*-heterocyclic carbene ligands was achieved by the deprotonation of the corresponding imidazolium, benzimidazolium or imidazolinium salts with potassium *tert*-butoxide in methanol. Subsequent addition of the cyclometalated gold(III) precursor, [Au(RC^N^CR)Cl], and heating under reflux led to the successful incorporation of the NHC ligands into the gold(III) moiety. Metathesis with tetra-*n*-butylammonium hexafluorophosphate afforded the crude products as yellow solids. Subsequent recrystallization from slow diffusion of diethyl ether vapor into a concentrated dichloromethane solution of the complex resulted in the isolation of the desired product as yellow crystals. All complexes are found to be air- and heat-stable. Compared to the chlorogold(III) precursor complexes, the organogold(III) complexes incorporated with NHC ligands were found to be much more soluble in common organic solvents such as dichloromethane. The identities of all the complexes, namely, **1**−**11**, have been confirmed by ^1H NMR spectroscopy, FAB- or ESI-mass spectrometry and satisfactory elemental analyses. The crystal structures of all complexes (with the exception of **4** and **8**) have also been determined by X-ray crystallography.

X-Ray Crystal Structures. Single crystals of **1**−**3**, **5**−**7** and **9**−**11** were obtained by slow diffusion of diethyl ether vapor into a dichloromethane solution of the respective complexes (for **1**−**3**, **6**, **7**, **9** and **10**) or by layering of *n*-hexane onto a concentrated dichloromethane solution of the complexes (for **5** and **11**), and their structures were solved by X-ray crystallography. Crystal structure determination data are summarized in Table S1 in Supporting Information. The selected bond distances and bond angles, as well as selected intermolecular parameters, are tabulated in Tables S2 and S3 in Supporting Information, respectively. The perspective views of the crystal structures of **1**, **3**, **6** and **11** are depicted in Figure 1, whereas those of **2**, **5**, **7**, **9** and **10** are in Figure S1 in Supporting Information. In each case, the gold(III) metal center coordinates to the bis-cyclometalated tridentate RC^N^CR pincer ligand with the remaining site occupied by a *N*-heterocyclic carbene ligand to give a distorted square-planar geometry, characteristic of d^8 metal complexes. The C−Au−C and C−Au−N angles of 160.8−163.5° and 79.2−83.0° about the gold(III) metal center deviate from the idealized values of 180° and 90°, respectively, as a result of the restricted bite angle of the tridentate RC^N^CR

(12) Barnard, P. J.; Wedlock, L. E.; Baker, M. V.; Berners-Price, S. J.; Joyce, D. A.; Skelton, B. W.; Steer, J. H. *Angew. Chem., Int. Ed.* **2006**, *45*, 5966–5970.
(13) Yam, V. W.-W.; Lee, J. K.-W.; Ko, C.-C.; Zhu, N. *J. Am. Chem. Soc.* **2009**, *131*, 912–913.
(14) (a) Yam, V. W.-W.; Cheng, E. C.-C. *Top. Curr. Chem.* **2007**, *281*, 269–309. (b) Yam, V. W.-W.; Cheng, E. C.-C. *Chem. Soc. Rev.* **2008**, *37*, 1806–1813.
(15) Vogler, A.; Kunkely, H. *Coord. Chem. Rev.* **2001**, *219*−*221*, 489–507.
(16) Yam, V. W.-W.; Choi, S. W.-K.; Lai, T.-F.; Lee, W.-K. *J. Chem. Soc., Dalton Trans.* **1993**, 1001–1002.
(17) (a) Wong, K.-H.; Cheung, K.-K.; Chan, M. C.-W.; Che, C.-M. *Organometallics* **1998**, *17*, 3505–3511. (b) Yam, V. W.-W.; Wong, K. M.-C.; Hung, L.-L.; Zhu, N. *Angew. Chem., Int. Ed.* **2005**, *44*, 3107–3110. (c) Wong, K. M.-C.; Zhu, X.; Hung, L.-L.; Zhu, N.; Yam, V. W.-W.; Kwok, H.-S. *Chem. Commun.* **2005**, 2906–2908. (d) Wong, K. M.-C.; Hung, L.-L.; Lam, W. H.; Zhu, N.; Yam, V. W.-W. *J. Am. Chem. Soc.* **2007**, *129*, 4350–4365.
(18) (a) Urbano, J.; Hormigo, A. J.; de Frémont, P.; Nolan, S. P.; Díaz-Requejo, M. M.; Pérez, P. J. *Chem. Commun.* **2008**, 759–761. (b) de Frémont, P.; Singh, R.; Stevens, E. D.; Petersen, J. L.; Nolan, S. P. *Organometallics* **2007**, *26*, 1376–1385.
(19) Jothibasu, R.; Huynh, H. V.; Koh, L. L. *J. Organomet. Chem.* **2008**, *693*, 374–380.

Chart 1

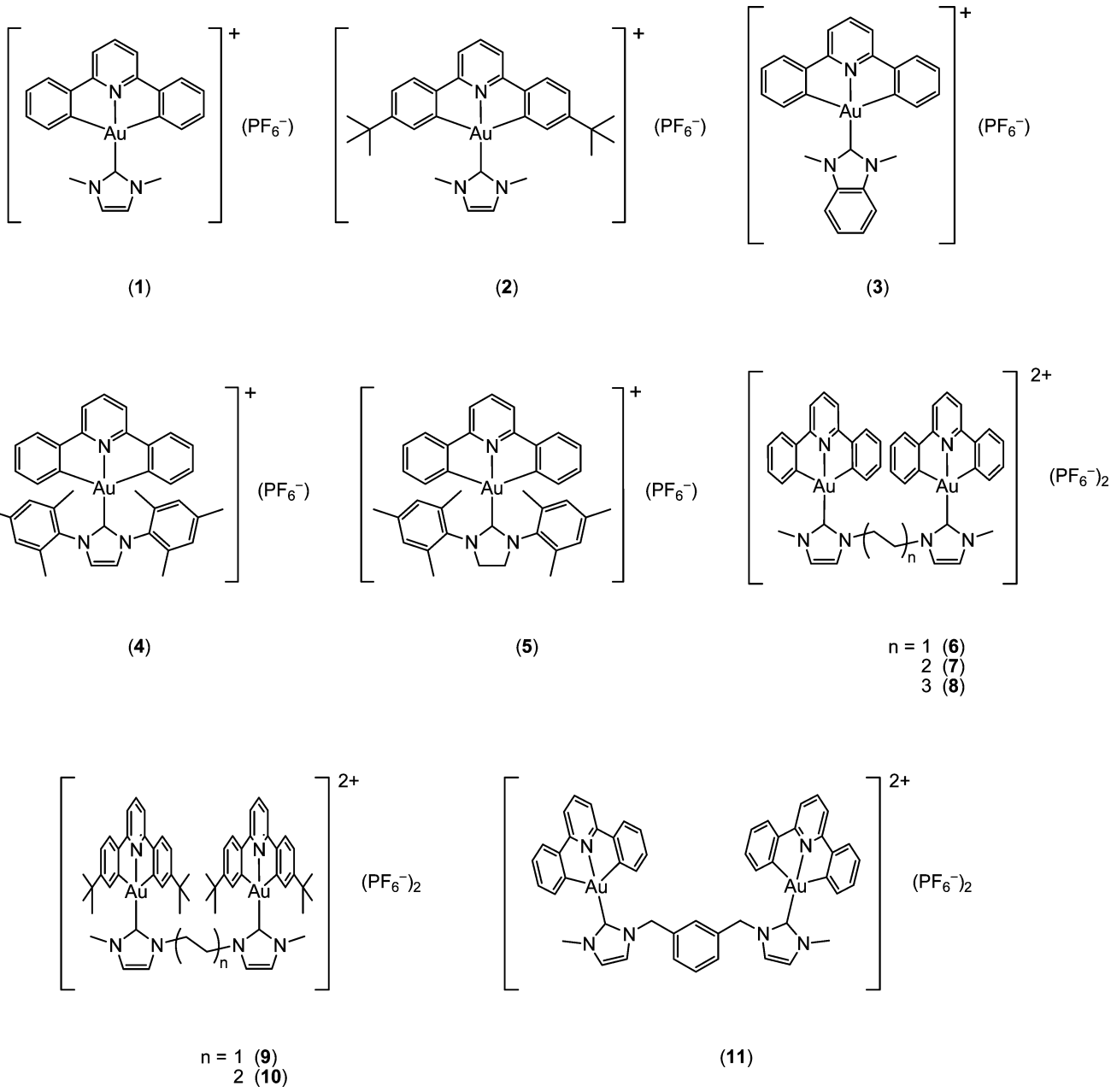

ligand. The [Au(RC^N^CR)] motif is essentially coplanar, and the Au−C (2.055−2.151 Å) and Au−N (1.966−2.020 Å) bond distances are similar to those found in related bis-cyclometalated alkynylgold(III) complexes.[17b–d]

With the attachment of the cyclometalating RC^N^CR ligand, the Au−C(NHC) distances are found to range from 1.967 to 2.017 Å, which are slightly shorter than those of [(NHC)$AuBr_3$] and *trans*-[AuI_2(^{i}Pr_2-bimy)$_2$]BF_4 reported in the literature (2.009−2.052 Å).[18,19] The planes of the cyclometalating RC^N^CR ligand and the auxiliary NHC ligand are not coplanar to each other. They are arranged in a twisted manner with respect to each other, with the interplanar angles between the [Au(RC^N^CR)] and NHC moieties varying from 53.605° to 81.975°.

Since the shortest Au···Au distances (4.530−9.364 Å) between adjacent molecules or within a molecule are found to be longer than the sum of van der Waals radii for two gold(III) centers, no significant Au···Au interactions occur in the crystal lattices of the complexes. On the other hand, appreciable $\pi-\pi$ stacking interactions can be revealed by the shortest interplanar distances between the [Au(RC^N^CR)] moieties in most of the complexes, with the smallest value being 3.42 Å in **6** (Table S3 in Supporting Information). The packing arrangements of the complexes vary from one structure to another. Figure 2 depicts the crystal packing diagrams of **3** and **6**, whereas those of **1**, **2**, **5**, **7** and **9**−**11** are shown in Figure S2 in Supporting Information. For crystals of **1**, **3**, **5**−**7** and **11**, the complex molecules are stacked into an extended columnar array with identical Au···Au and $\pi-\pi$ separations between them, while the [Au(RC^N^CR)] motifs are partially stacked with different extents of aromatic overlapping. The [Au(RC^N^CR)] moieties are stacked in a variety of manners and are shifted laterally with respect to each other. The mononuclear complex

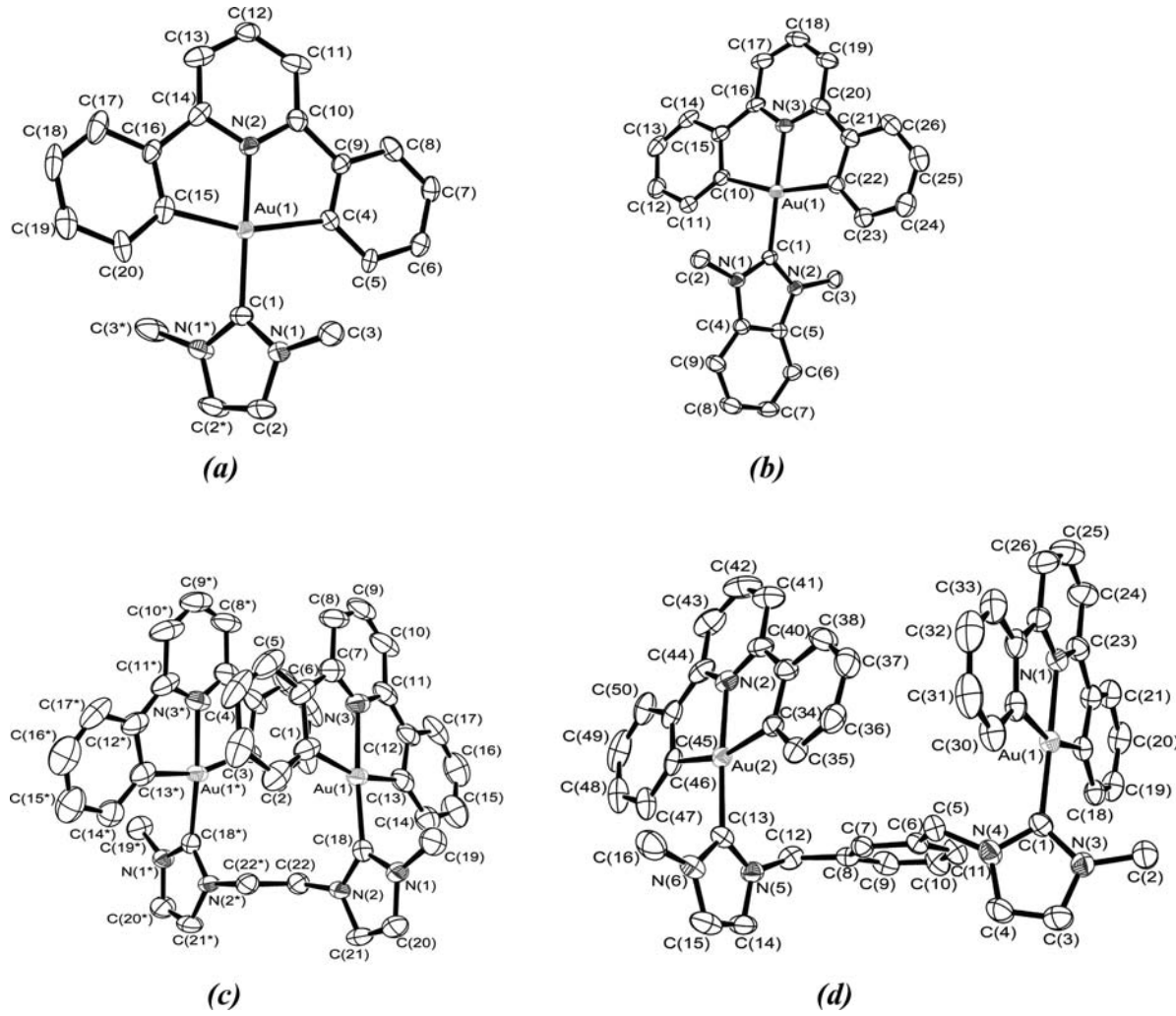

Figure 1. Perspective drawings of the complex cations of **1** (a), **3** (b), **6** (c), and **11** (d) with atomic numbering scheme. Hydrogen atoms and solvent molecules are omitted for clarity. Thermal ellipsoids are drawn at the 30% probability level.

1 is arranged in a head-to-tail fashion and exhibits intermolecular $\pi-\pi$ interactions. The introduction of bulky *tert*-butyl groups onto the phenyl rings of the RC^N^CR ligand has caused distortion in the crystal packing, resulting in a more irregular arrangement in **2**, as well as the absence of $\pi-\pi$ interactions. Complexes **3** and **5** show different configurations in their packing arrangements, in which the former shows stacking arrangements with the benzimidazole planes parallel to each other with slight intermolecular overlapping of [Au(RC^N^CR)] moieties, whereas the latter is arranged in a head-to-head fashion with no $\pi-\pi$ stacking.

For the dinuclear complexes, **6** and **7** exhibit similar crystal packing arrangements in a head-to-tail manner and are both stacked into extended columnar arrays. Significant intra- and intermolecular $\pi-\pi$ interactions are observed in complex **6**, mainly due to the short -CH_2CH_2- bridging NHC ligand. On the other hand, with an increased length of the carbon bridge, no intramolecular $\pi-\pi$ interactions is seen in **7**, but intermolecular $\pi-\pi$ interactions can still be observed between the molecules. As for **2**, the introduction of sterically hindered *tert*-butyl groups into the RC^N^CR ligand has led to substantial changes in the crystal packing of dinuclear complexes **9** and **10** compared to their unsubstituted RC^N^CR analogs, mainly due to the mutual repulsion between the sterically bulky *tert*-butyl groups. For crystals of **9**, the adjacent molecules are arranged in an orthogonal fashion with respect to each other. Neither intra- nor intermolecular $\pi-\pi$ interactions can be observed in **9**. Although there remain some intermolecular $\pi-\pi$ interactions in the crystal packing of **10** in the presence of bulky *tert*-butyl groups, the molecules are arranged quite differently from those of **7**. Complex **10** is arranged in a dimeric configuration instead of an extended columnar array. For crystals of **11**, the [Au(RC^N^CR)] moieties of adjacent molecules are aligned in parallel to each other with significant intermolecular $\pi-\pi$ interactions, and the bridging phenyl rings of the NHC ligands are also arranged in a parallel fashion.

Electrochemistry. The cyclic voltammograms of **1**−**11** in dichloromethane (0.1 mol dm^{-3} $^nBu_4NPF_6$) generally show one quasi-reversible reduction couple at −1.25 to −1.44 V vs SCE and no oxidation waves. The electrochemical data are summarized in Table 1, and the representative cyclic voltammograms of **1**, **6**, **7** and **8** are shown in Figure 3. Based on the fact that all complexes showed potentials for the reduction couple at similar region, the reduction process is assigned as the ligand-centered reduction of the RC^N^CR ligand. Comparison of the reduction potentials for **1** and **3**−**5** showed that the potentials for the reduction wave are rather insensitive to the nature of the NHC ligand. The occurrence of this reduction at more negative potential in **2**, **9** and **10**, relative to **1**, **6** and **7**, respectively, is also in line with this assignment, since the

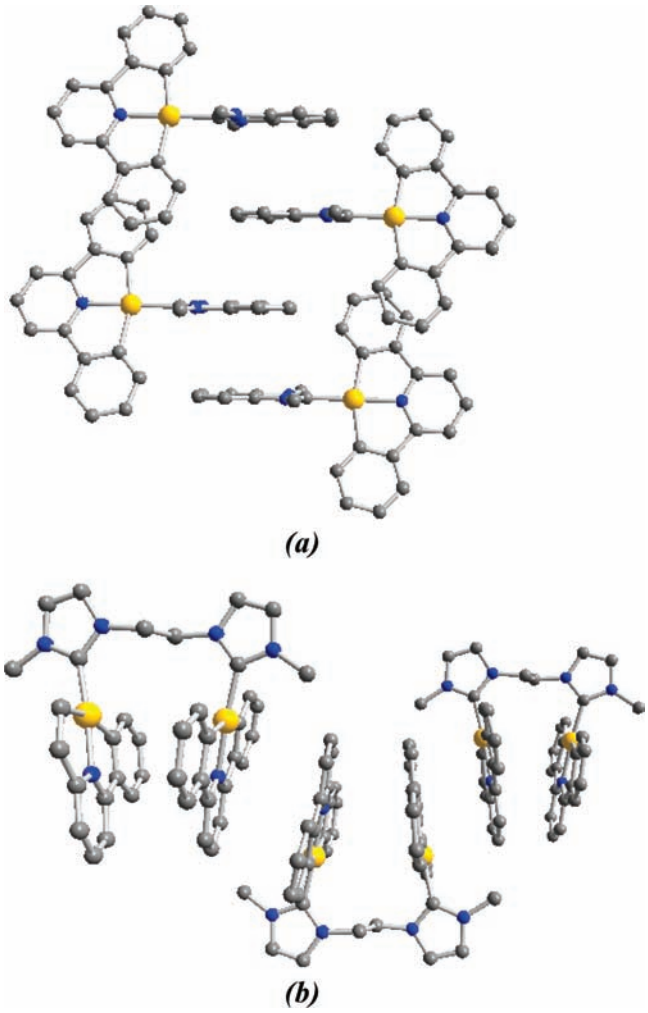

Figure 2. Crystal packing diagrams of the complex cations of **3** (a) and **6** (b).

Table 1. Electrochemical Data for **1**−**11**[a]

complex	reduction $E_{1/2}$, V vs SCE[b]
1	−1.39
2	−1.43
3	−1.34
4	−1.40
5	−1.39
6	−1.25,−1.50
7	−1.30,−1.37
8	−1.38
9	−1.42
10	−1.44
11	−1.36

[a] In dichloromethane solution with 0.1 M ^{n}Bu$_4$NPF$_6$ (TBAH) as supporting electrolyte at room temperature; scan rate 100 mV s^{-1}. [b] $E_{1/2} = (E_{pa} + E_{pc})/2$; E_{pa} and E_{pc} are peak anodic and peak cathodic potentials, respectively.

electron-rich *tert*-butyl substituents on the RC^N^CR ligand in **2**, **9** and **10** would destabilize the π^*(RC^N^CR) orbital, reducing the ease of reduction to give more negative potentials at −1.42 to −1.44 V vs SCE.

The dinuclear complexes **7**, **8** and **11** are found to show reduction potentials similar to those of the corresponding mononuclear complexes **1** and **3**−**5**. The *tert*-butyl-substituted complexes also showed similar observations, where the mononuclear complex **2** and the dinuclear complexes **9** and **10** showed almost identical reduction potential values.

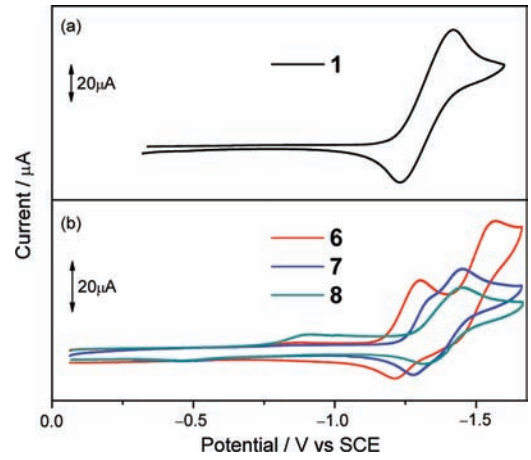

Figure 3. Cyclic voltammograms of (a) **1**, (b) **6**, **7** and **8** in CH_2Cl_2 (0.1 mol dm^{-3} ^{n}Bu$_4$NPF$_6$).

It is interesting to note that complexes **6** and **7** showed two reduction couples at less negative reduction potentials compared to **1** and **8**, with **6** being most obvious. The observation of a less negative potential of −1.25 V for **6** is probably attributed to the presence of intramolecular $\pi-\pi$ stacking within the molecule, as shown by the short interplanar separations between the [Au(RC^N^CR)] moieties of 3.64 Å within the dinuclear molecule. The two well-separated reduction couples are indicative of the occurrence of significant electronic communication in **6**. As the bridging chain length increases, the extent of electronic communication diminishes. Some degree of electronic communication could still be observed in the cyclic voltammogram of **7**, but it became unobservable in **8**. At first glance, using the potential separation ΔE value of 250 mV, a comproportionation constant (K_c) value of 16815 was obtained for **6**, whereas **7** showed a ΔE of 70 mV ($K_c = 15$), which suggests a larger extent of delocalization and hence a higher stability of the mixed valence state in **6**.[20] Alternatively, the observation of two reduction couples in the dinuclear complexes **6** and **7** could also result from the $\pi-\pi$ interaction between adjacent RC^N^CR moieties in **6** and **7**, which would cause a splitting of the π^* orbital-based LUMO, giving rise to two closely lying π^* orbitals, with the stabilization of the lower-lying π^* orbital (new LUMO), rendering the first reduction process to occur more readily. We are in favor of the latter assignment, since a much less negative first reduction potential was observed in **6**, which is not usually observed in other mixed-valence systems where a more negative first reduction potential is usually obtained.[21] On the other hand, dinuclear complexes **9** and **10** with *tert*-butyl-substituted RC^N^CR ligands failed to show such a phenomenon, with no splitting of the reduction couple being observable. This is because the sterically bulky *tert*-butyl groups do not allow such $\pi-\pi$ interaction to occur. As a result, complexes **9** and **10** exhibit less ordered packing arrangements compared to **6** and **7**, and no intramolecular $\pi-\pi$ stacking can be observed in **9** and **10**, as revealed by the larger interplanar separations between the [Au(RC^N^CR)] moieties within the molecule.

(20) Browne, W. R.; Hage, R.; Vos, J. G. *Coord. Chem. Rev.* **2006**, *250*, 1653–1668.
(21) Hua, D. H.; McGill, J. W.; Lou, K.; Ueki, A.; Helfrich, B.; Desper, J.; Zanello, P.; Cinquantini, A.; Corsini, M.; Fontani, M. *Inorg. Chim. Acta* **2003**, *350*, 259–265.

Table 2. Photophysical Data for **1**−**11**

	absorption[a]	emission		
complex	λ_{max}/nm (ε_{max}/dm^{3}mol^{-1}cm^{-1})	medium (T/K)	λ_{max}/nm (τ_0/μs)	Φ_{em}[b]
1	369 (2995)	CH_2Cl_2 (298)[c]	479, 511, 548 (0.6)	3.9×10^{-3}
	386 (4695)	glass (77)[c,d]	471, 503, 537 (430)	
	406 (4305)			
2	378 (3655)	CH_2Cl_2 (298)[c]	489, 521, 560 (0.6)	9.6×10^{-3}
	396 (6565)	glass (77)[c,d]	479, 513, 549 (476)	
	418 (6375)			
3	369 (3075)	CH_2Cl_2 (298)[c]	480, 511, 548 (0.6)	3.5×10^{-3}
	387 (4855)	glass (77)[c,d]	470, 503, 535 (396)	
	407 (4445)			
4	370 (2815)	CH_2Cl_2 (298)	non-emissive	
	388 (4525)	glass (77)[c,d]	475, 507, 540 (406)	
	408 (4340)			
5	370 (2510)	CH_2Cl_2 (298)	non-emissive	
	386 (4130)	glass (77)[c,d]	473, 508, 540 (415)	
	406 (3920)			
6	373 (4640)	CH_2Cl_2 (298)[c]	487, 520, 552 (2.6)	7.7×10^{-3}
	391 (7240)	glass (77)[c,d]	474, 511, 544 (439)	
	411 (6400)			
7	370 (5270)	CH_2Cl_2 (298)[c]	490, 520, 555 (0.6)	5.1×10^{-3}
	386 (8255)	glass (77)[c,d]	472, 504, 537 (405)	
	406 (7490)			
8	370 (4890)	CH_2Cl_2 (298)[c]	490, 521, 555 (0.6)	2.6×10^{-3}
	386 (7460)	glass (77)[c,d]	472, 507, 541 (402)	
	406 (6835)			
9	382 (6045)	CH_2Cl_2 (298)[c]	493, 523, 563 (10.3)	8.2×10^{-3}
	400 (10395)	glass (77)[c,d]	481, 515, 548 (531)	
	420 (10275)			
10	380 (6590)	CH_2Cl_2 (298)[c]	490, 521, 558 (4.3)	1.7×10^{-2}
	398 (10850)	glass (77)[c,d]	481, 514, 547 (486)	
	418 (10415)			
11	370 (5460)	CH_2Cl_2 (298)[c]	491, 521, 554 (0.4)	2.1×10^{-3}
	386 (8115)	glass (77)[c,d]	474, 508, 537 (405)	
	406 (7215)			

[a] In dichloromethane at 298 K. [b] Luminescence quantum yield, measured at room temperature using quinine sulfate as a standard. [c] Vibronic-structured emission band. [d] In EtOH−MeOH−CH_2Cl_2 (40:10:1 v/v).

UV−Vis Absorption Spectroscopy. The UV−visible absorption spectra of complexes **1**−**11** in dichloromethane at 298 K exhibit an intense absorption band at ca. 310 nm and a moderately intense vibronic-structured band at 370−410 nm with extinction coefficients (ε) on the order of 10^4 dm^3 mol^{-1} cm^{-1}. These results are found to resemble those of other cyclometalated alkynylgold(III) complexes previously reported.[17b–d] The photophysical data of **1**−**11** are summarized in Table 2, and the corresponding electronic absorption spectra of **1**, **2**, **4**, **6**, **7**, **9** and **10** are depicted in Figure 4. For mononuclear complexes **1**, **3**, **4** and **5**, the absorption energy of the low-energy vibronic band at ca. 370−410 nm is found to be rather insensitive to the nature of the NHC ligand. Complexes **4** and **5** are found to exhibit comparatively smaller extinction coefficients. The vibrational progressional spacings of ca. 1200−1300 cm^{-1} are in close agreement with the skeletal vibrational frequency of the RC^N^CR ligand. This suggests an assignment of the low-energy vibronic band as a metal-perturbed $\pi \rightarrow \pi^*$ intraligand (IL) transition of the RC^N^CR ligand, probably involving some charge transfer character from the phenyl moiety to the pyridyl unit. Since the electron-donating *tert*-butyl groups on the phenyl rings would increase the energy of the HOMO π orbital that was more localized on the aryl ring, a narrowing of the HOMO−LUMO energy gap would result, leading to lower absorption energies for **2**, **9** and **10**.

The dinuclear complexes **6**−**10** generally showed larger extinction coefficients compared to the mononuclear counterparts **1** and **2** because the former have two Au(III)-RC^N^CR moieties per molecule involved in the electronic absorption. With the exception of **6**, the dinuclear complexes **7**, **8** and **11** showed nearly the same absorption maxima in the electronic absorption spectra. This is probably due to the presence of $\pi-\pi$ stacking in **6**, which resulted in a red shift in absorption energy. On the contrary, the dinuclear complexes **9** and **10** show absorption energies similar to that of **2**. In order to study the presence of intermolecular and/or intramolecular $\pi-\pi$ stacking in the dinuclear complexes, complexes **6**−**11** have all been subjected to concentration-dependence studies for both their electronic absorption and emission measurements. Three different concentrations of each complex solution, on the order of 10^{-5} to 10^{-3} M, have been prepared and used for the absorption measurements. In all cases, no concentration dependence was observed, showing that either no $\pi-\pi$ stacking in the complexes exists or any $\pi-\pi$ stacking that influences the photophysical properties would be intramolecular in nature. From the concentration-dependence studies, it was deduced that the red shift in **6** is due to the presence of significant intramolecular $\pi-\pi$ stacking interactions. Due to the shorter chain length of the bridging ligand in **6** compared to **7** and **8**, the interplanar separation of the RC^N^CR planes is intrinsically shorter in **6**, giving rise to much stronger $\pi-\pi$ interactions, leading to a smaller HOMO−LUMO energy gap that results in a red shift in absorption energy, and such $\pi-\pi$ interaction has also been confirmed by X-ray crystallographic studies.

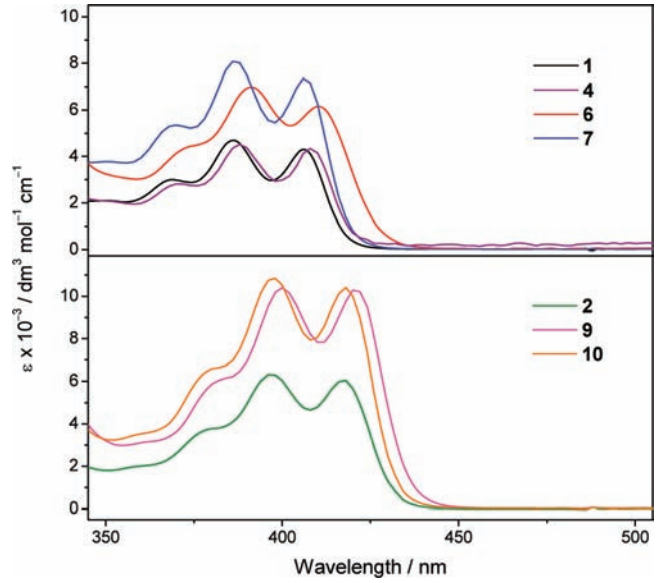

Figure 4. Electronic absorption spectra of **1**, **2**, **4**, **6**, **7**, **9** and **10** in CH_2Cl_2 at room temperature.

Luminescence Spectroscopy. This class of gold(III) compounds is found to exhibit strong luminescence. Their photoluminescence properties in dichloromethane solution at room temperature and in ethanol−methanol−dichloromethane (40:10:1 v/v) glass at 77 K have been studied. In dichloromethane solutions at 298 K, the gold(III) complexes, with the exception of **4** and **5**, exhibit moderately intense luminescence at 471−563 nm at room temperature. The photophysical data of **1**−**11** are tabulated in Table 2. In contrast to the chloro precursor complex, [Au(RC^N^CR)Cl], which is reported to be non-emissive at room temperature, incorporation of the strong σ-donating *N*-heterocyclic carbene ligands into gold(III) has led to the enhancement of the photoluminescence properties of these cyclometalated

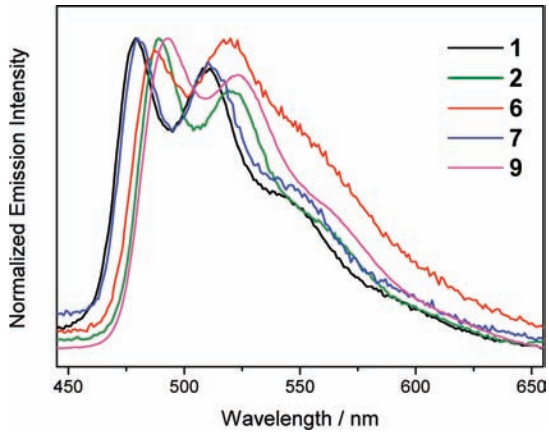

Figure 5. Emission spectra of **1**, **2**, **6**, **7** and **9** in degassed CH_2Cl_2 at room temperature.

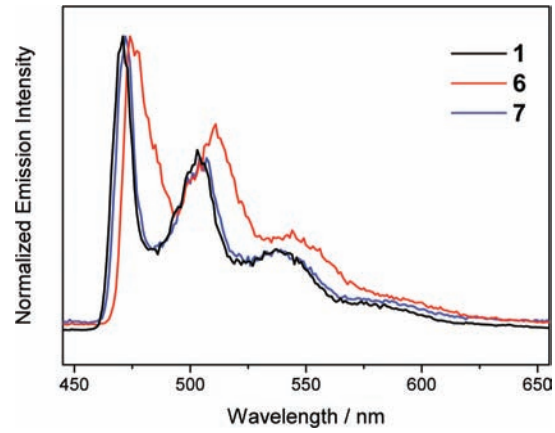

Figure 6. Emission spectra of **1**, **6** and **7** in low-temperature EtOH−MeOH−CH_2Cl_2 (40:10:1 v/v) glass at 77 K.

gold(III) complexes via the enlargement of the d-d ligand field splitting. This concept has also been demonstrated in other related alkynylgold(III) complexes, [Au(RC^N^CR)-(C≡C-R)].[17b–d] Figure 5 depicts the emission spectra of **1**, **2**, **6**, **7** and **9** in dichloromethane solution at room temperature. The emission lifetimes in the submicrosecond to microsecond range, together with the observed large Stokes shift, suggest that the emission is of triplet parentage.

Upon excitation at $\lambda \geq 350$ nm, mononuclear complexes **1** and **3** showed nearly identical spectra with a vibronic-structured emission band at ca. 511 nm in dichloromethane solution at room temperature. This suggests that increased conjugation in **3** has caused no significant change in the emission energies. The vibrational progressional spacings of about 1300 cm^{-1} are characteristic of the C═C and C═N stretching frequencies of the tridentate ligand, indicative of the involvement of the tridentate RC^N^CR ligand in the excited-state origin. The luminescence is assigned as originating from a metal-perturbed $^3[\pi-\pi^*$ (RC^N^CR)] intraligand state. Similar assignment has also been made in related mononuclear cyclometalated gold(III) complexes.[17] As in the electronic absorption study, the emission band of **2** is red-shifted as a result of the attachment of the electron-donating *tert*-butyl groups on the phenyl rings, giving rise to the narrower HOMO−LUMO gap due to the charge transfer character from the aryl ring to the pyridine moiety of the RC^N^CR ligand-centered excited state. Despite the close analogy of tertiary phosphines to NHC ligands, it is noteworthy that incorporation of NHC as auxiliary ligands has caused much more substantial enhancement in the photoluminescence properties of gold(III) complexes when compared to the related phosphine-containing gold(III) complexes, [Au(C^N^C)PPh_3]-ClO_4, which have been reported as non-emissive in fluid solution at room temperature and only emissive at low temperature.[17a] On the other hand, **4** and **5** were found to be non-emissive in dichloromethane solution at room temperature, probably due to the presence of electron-rich mesityl groups, which may lead to quenching of the photoluminescence.

Emission bands of dinuclear complexes **6**−**11** were found to be concentration-independent in the range 3.68×10^{-5} to 2.25×10^{-3} mol dm^{-3}. All the dinuclear complexes were observed to exhibit emission maxima at longer wavelengths compared to their mononuclear counterparts. Similar observations have also been observed in the emission of related phosphine-containing gold(III) complexes in acetonitrile glass at 77 K.[17a] Complexes **7**, **8** and **11** showed nearly identical emission spectra, with emission maxima at ca. 521 nm, whereas the *tert*-butyl-substituted complexes **9** and **10** showed the most red-shifted emission bands due to the attachment of electron-rich *tert*-butyl groups on the phenyl rings of the tridentate ligand. Parallel to the electronic absorption studies, complex **6** was observed to show a slight red shift relative to that of **7** and **8**, with much broader bands that can be attributed to result from the intramolecular $\pi-\pi$ stacking interactions of the RC^N^CR ligands. Ligand-centered phosphorescence has also been reported in other organic π-stacked systems in the presence of heavy metal centers.[22]

For emission studies in low-temperature glass, all of the complexes show similar vibronic-structured emission bands with an emission energy similar to that observed in dichloromethane solution. The emission spectra of **1**, **6** and **7** in low-temperature EtOH−MeOH−CH_2Cl_2 (40:10:1 v/v) glass at 77 K are shown in Figure 6. These emission bands are similarly assigned as derived from intraligand states of the cyclometalating RC^N^CR ligand. As in dichloromethane solution, the ethanol−methanol−dichloromethane glass emission also exhibited vibrational progressional spacings of 1200−1300 cm^{-1}, which agree well with the C═C and C═N stretching modes of the RC^N^CR ligands. In contrast to the solution emission, which showed short lifetimes in the range of 0.6−10.3 μs, all complexes show much longer lifetimes in the glass emission of at least 396 μs. Despite their lack of photoluminescence at room temperature in dichloromethane solution, complexes **4** and **5** were found to be emissive in low-temperature glass, with emission maxima at slightly longer wavelengths compared to **1** and **3**. As in the solution emission studies, the dinuclear complexes show a red shift in their emission maxima compared to the mononuclear analogs, with complex **6** showing the most substantial shift.

Conclusion

A novel class of luminescent *N*-heterocyclic carbene-containing gold(III) complexes has been synthesized and characterized. The X-ray crystal structures of most of the complexes have been determined, and intramolecular $\pi-\pi$ stacking interactions were apparent between adjacent RC^N^CR planes in **6**. Electrochemical studies reveal a ligand-centered reduction originated from

(22) (a) Omary, M. A.; Mohamed, A. A.; Rawashdeh-Omary, M. A.; Fackler, J. P., Jr. *Coord. Chem. Rev.* **2005**, *249*, 1372–1381. (b) Haneline, M. R.; Tsunoda, M.; Gabbaï, F. P. *J. Am. Chem. Soc.* **2002**, *124*, 3737–3742. (c) Omary, M. A.; Kassab, R. M.; Haneline, M. R.; Elbjeirami, O.; Gabbaï, F. P. *Inorg. Chem.* **2003**, *42*, 2176–2178.

the RC^N^CR moieties with no oxidation waves. It is interesting to note that dinuclear complex **6**, which showed significant intramolecular $\pi-\pi$ stacking in its X-ray crystal structure, exhibited two distinct reduction couples, with the first reduction occurring at less negative potential. Such observation is tentatively correlated to the presence of intramolecular $\pi-\pi$ interaction in **6**, which results in the splitting of the π^* orbital-based LUMO, thereby giving rise to a new LUMO of lower energy such that the first reduction process can occur more readily. The electronic absorption and emission properties of the complexes have also been studied. In dichloromethane solution at room temperature, the low-energy absorption bands are ascribed to the intraligand $\pi-\pi^*$ transition, with mixing of a charge transfer character from the aryl ring to the pyridine moiety of the cyclometalating RC^N^CR ligand. For the emission studies in dichloromethane solution at room temperature and in low-temperature glass, vibronic-structured emission bands were observed, which are tentatively assigned as originating from intraligand $\pi-\pi^*$ states with an aryl to pyridine charge transfer character of the RC^N^CR cyclometalating ligand. Although the photophysical properties of this series of complexes are rather insensitive to the nature of the NHC auxiliary ligands, the successful incorporation of NHC ligands into the gold(III) metal center was found to enhance their luminescence properties. Moreover, the dinuclear complexes containing bridging NHC ligand with short spacer exhibited interesting luminescence and electrochemical properties of π-stacked systems.

Experimental Section

Materials and Reagents. Potassium *tert*-butoxide was purchased from Merck. Potassium tetrachloroaurate(III) was purchased from ChemPur. Tetra-*n*-butylammonium hexafluorophosphare was obtained from Strem, and 1,3-bis(2,4,6-trimethylphenyl)imidazolinium chloride and 1,3-bis(2,4,6-trimethylphenyl)imidazolium chloride were from Aldrich. [Hg(C^N^CH)Cl] (HC^N^CH = 2,6-diphenylpyridine),[17] [Hg(′BuC^N^C′BuH)Cl] (H′BuC^N^C′BuH = 2,6-bis(4-*tert*-butylphenyl)pyridine),[17] [Au(C^N^C)Cl],[17] [Au(′BuC^N^C′Bu)Cl],[17] 2,6-bis(4-*tert*-butylphenyl)pyridine,[17] 1,3-dimethylimidazolium iodide,[23] 1,2-bis(3-methylimidazolium-1-yl)ethane chloride,[24] 1,4-bis(3-methylimidazolium-1-yl)-butane chloride,[24] 1,6-bis(3-methylimidazolium-1-yl)hexane chloride,[24] 1,3-dimethyl-benzimidazolium iodide[25] and 2,6-bis(1-methyl-imidazolium-3-yl)pyridine dibromide[26] were prepared according to literature procedures. All solvents were purified and distilled using standard procedures before use. All other reagents were of analytical grade and used as received. Tetra-*n*-butylammonium hexafluorophosphate (Aldrich) was recrystallized twice from absolute ethanol before use.

Physical Measurements and Instrumentation. UV−Vis spectra were obtained on a Hewlett-Packard 8452A diode array spectrophotometer. ^{1}H NMR spectra were recorded on a Bruker DPX-300 (300 MHz) or Bruker DPX-400 (400 MHz) Fourier transform NMR spectrometer with chemical shifts recorded relative to tetramethylsilane (Me_4Si). Positive FAB mass spectra were recorded on a Finnigan MAT95 mass spectrometer, and ESI mass spectra were recorded on a Finnigan LCQ mass spectrometer. Elemental analyses for the metal complexes were performed on the Carlo Erba 1106 elemental analyzer at the Institute of Chemistry, Chinese Academy of Sciences in Beijing. Steady-state excitation and emission spectra were recorded on a Spex Fluorolog-2 model F111 fluorescence spectrofluorometer equipped with a Hamamatsu R-928 photomultiplier tube. All solutions for photophysical studies were prepared under a high vacuum in a 10-cm^3 round-bottomed flask equipped with a side arm 1-cm fluorescence cuvette and sealed from the atmosphere by a Rotaflo HP6/6 quick-release Teflon stopper. Solutions were rigorously degassed on a high-vacuum line in a two-compartment cell with no less than four successive freeze−pump−thaw cycles. Photophysical measurements in low-temperature glass were carried out with the sample solution loaded in a quartz tube inside a quartz-walled Dewar flask. Liquid nitrogen was placed into the Dewar flask for low temperature (77 K) photophysical measurements. Excited-state lifetimes of solution samples were measured using a conventional laser system. The excitation source used was the 355-nm output (third harmonic, 8 ns) of a Spectra-Physics Quanta-Ray Q-switched GCR-150 pulsed Nd:YAG laser (10 Hz). Luminescence quantum yields were measured by the optical dilute method reported by Demas and Crosby.[27a] A degassed aqueous solution of quinine sulfate in 1.0 N sulfuric acid ($\Phi = 0.546$, excitation wavelength at 365 nm) was used as the reference and corrected for the refractive index of the solution.[27b]

Cyclic voltammetric measurements were performed by using a CH Instruments, Inc. model CHI 600A electrochemical analyzer. The electrolytic cell used was a conventional three-compartment cell. Electrochemical measurements were performed in dichloromethane solutions with 0.1 M ^{n}Bu$_4$NPF$_6$ (TBAH) as supporting electrolyte at room temperature. The reference electrode was a Ag/$AgNO_3$ (0.1 M in acetonitrile) electrode, and the working electrode was a glassy carbon electrode (CH Instruments, Inc.) with a platinum wire as the counter electrode. The working electrode surface was first polished with a 1-μm alumina slurry (Linde), followed by a 0.3-μm alumina slurry, on a microcloth (Buehler Co.). Treatment of the electrode surfaces was as reported previously.[28a] The ferrocenium/ferrocene couple ($FeCp_2^{+/0}$) was used as the internal reference.[28b] All solutions for electrochemical studies were deaerated with prepurified argon gas just before measurements.

Crystal Structure Determination. Single crystals of **1**−**3**, **5**−**7** and **9**−**11** suitable for X-ray diffraction studies were grown by slow diffusion of diethyl ether vapor into a dichloromethane solution of the complexes (for **1**−**3**, **6**, **7**, **9** and **10**) or by layering of *n*-hexane onto a concentrated dichloromethane solution (for **5** and **11**) of the complexes. The X-ray diffraction data were collected either on a MAR diffractometer with a 300 nm image plate detector (for **1**, **6** and **7**) or on a Bruker Smart CCD 1000 (for **2**, **3**, **5** and **9**−**11**), both using graphite monochromatized Mo-Kα radiation (λ = 0.71073 Å). The images were interpreted and intensities were integrated using DENZO program.[29] The structure was solved by direct methods employing the SHELXS-97 program.[30] Full-matrix least-squares refinement on F^2 was used in the structure refinement. The positions of H atoms were calculated on the basis of the riding mode with thermal parameters equal to 1.2 times those of the associated C atoms and participated in the calculation of final *R*-indices. In the final stage of least-squares refinement, all non-hydrogen atoms were refined anisotropically.

(23) Benac, B. L.; Burgess, E. M.; Arduengo, A. J., III *Org. Synth.* **1986**, *64*, 92–95.
(24) Liu, Q.; van Rantwijk, F.; Sheldon, R. A. *J. Chem. Technol. Biotechnol.* **2006**, *81*, 401–405.
(25) Bostai, B.; Novák, Z.; Bényei, A. C.; Kotchy, A. *Org. Lett.* **2007**, *9*, 3437–3439.
(26) Chen, J. C. C.; Lin, I. J. B. *J. Chem. Soc., Dalton Trans.* **2000**, 839–840.
(27) (a) Demas, J. N.; Crosby, G. A. *J. Phys. Chem.* **1971**, *75*, 991–1024. (b) van Houten, J.; Watts, R. *J. Am. Chem. Soc.* **1976**, *98*, 4853–4858.
(28) (a) Che, C. M.; Wong, K. Y.; Anson, F. C. *J. Electroanal. Chem. Interfacial Electrochem.* **1987**, *226*, 211–226. (b) Connelly, N. G.; Geiger, W. E. *Chem. Rev.* **1996**, *96*, 877–910.
(29) Written with the cooperation of the program authors: Otwinowski, Z.; Minor, W.; Gewith, D. *DENZO: The HKL Manuals−A Description of Programs DENZO, XDISPLAYF, and SCALEPACK*; Yale University: New Haven, CT, 1995.
(30) Sheldrick, G. M. *SHELXS 97: Programs for Crystal Structure Analysis (release 97-2)*; University of Göttingen: Göttingen, Germany, 1997.

Syntheses of NHC-Containing Gold(III) Complexes. [Au(C^N^C)(IMe)]PF_6 1. (IMe = 1,3-dimethylimidazol-2-ylidene) A mixture of 1,3-dimethylimidazolium iodide (73 mg, 0.326 mmol) and potassium *tert*-butoxide (61 mg, 0.545 mmol) in methanol (60 mL) was heated to reflux for 30 min, after which [Au(C^N^C)Cl] (100 mg, 0.217 mmol) was added to give a pale yellow suspension. The resulting mixture was heated to reflux for 12 h. After cooling to room temperature, the reaction mixture was concentrated and subjected to a metathesis reaction with ammonium hexafluorophosphate in methanol to give a yellow solid. The crude product was collected by filtration and washed with diethyl ether. Subsequent recrystallization from slow diffusion of diethyl ether vapor into the concentrated dichloromethane or chloroform solution gave the titled complex as yellow crystals. Yield: 76 mg (53%). ^{1}H NMR (400 MHz, DMSO-d_6, 298 K): δ 3.83 (s, 6H, $-CH_3$), 6.94 (d, 2H, J = 7.1 Hz, imidazolyl of NHC), 7.31 (t, 2H, J = 7.5 Hz, phenyl of C^N^C), 7.37 (t, 2H, J = 7.5 Hz, phenyl of C^N^C), 7.84 (s, 2H, phenyl of C^N^C), 7.99 (d, 2H, J = 7.5 Hz, phenyl of C^N^C), 8.06 (d, 2H, J = 8.0 Hz, pyridyl of C^N^C), 8.27 (t, 1H, J = 8.0 Hz, pyridyl of C^N^C). Positive FAB-MS: m/z 523 $[M - PF_6]^+$. Elemental analyses calcd for $C_{22}H_{19}N_3PF_6Au \cdot 1/2(C_2H_5)_2O$ (found): C, 40.92 (40.67); H, 3.43 (3.21); N, 5.97 (6.09).

[Au(^{t}BuC^N^C^{t}Bu)(IMe)]PF_6 2. (IMe = 1,3-dimethylimidazol-2-ylidene) Synthesized according to a procedure similar to that of **1** except [Au(^{t}BuC^N^C^{t}Bu)Cl] (124 mg, 0.216 mmol) was used in place of [Au(C^N^C)Cl]. Yellow crystals of **2** were obtained. Yield: 95 mg (56%). ^{1}H NMR (400 MHz, DMSO-d_6, 298 K): δ 1.21 (s, 18H, ^{t}Bu), 3.85 (s, 6H, $-CH_3$), 6.90 (s, 2H, imidazolyl of NHC), 7.38 (d, 2H, J = 8.0 Hz, phenyl of C^N^C), 7.90 (m, 4H, phenyl of C^N^C), 7.96 (d, 2H, J = 8.0 Hz, pyridyl of C^N^C), 8.21 (t, 1H, J = 8.0 Hz, pyridyl of C^N^C). Positive FAB-MS: m/z 635 $[M - PF_6]^+$. Elemental analyses calcd for $C_{30}H_{35}N_3PF_6Au$ (found): C, 46.22 (46.20); H, 4.53 (4.55); N, 5.39 (5.44).

[Au(C^N^C)(BIMe)]PF_6 3. (BIMe = 1,3-dimethylbenzimidazol-2-ylidene) Synthesized according to a procedure similar to that of **1** except 1,3-dimethylbenzimidazolium chloride (89 mg, 0.325 mmol) was used in place of 1,3-dimethylimidazolium iodide. Yellow crystals of **3** were obtained. Yield: 108 mg (59%). ^{1}H NMR (300 MHz, DMSO-d_6, 298 K): δ 4.12 (s, 6H, $-CH_3$), 6.99 (d, 2H, J = 7.5 Hz, phenyl of C^N^C), 7.25 (t, 2H, J = 7.5 Hz, phenyl of C^N^C), 7.37 (t, 2H, J = 7.5 Hz, phenyl of C^N^C), 7.65 (m, 2H, benzimidazolyl of NHC), 8.00 (m, 4H, benzimidazolyl of NHC and phenyl of C^N^C), 8.09 (d, 2H, J = 8.1 Hz, pyridyl of C^N^C), 8.29 (t, 1H, J = 8.1 Hz, pyridyl of C^N^C). Positive ESI-MS: m/z 572 $[M - PF_6]^+$. Elemental analyses calcd for $C_{26}H_{21}N_3PF_6Au$ (found): C, 43.53 (43.21); H, 2.95 (2.95); N, 5.86 (5.87).

[Au(C^N^C)(IMes)]PF_6 4. (IMes = 1,3-dimesitylimidazol-2-ylidene) Synthesized according to a procedure similar to that of **1** except 1,3-bis(2,4,6-trimethylphenyl)imidazolium chloride (111 mg, 0.326 mmol) was used in place of 1,3-dimethylimidazolium iodide. Yellow crystals of **4** were obtained. Yield: 127 mg (67%). ^{1}H NMR (300 MHz, DMSO-d_6, 298 K): δ 2.15 (s, 6H, $-CH_3$), 2.25 (s, 12H, $-CH_3$), 6.96 (s, 4H -C_6H_2-), 7.22 (d, 2H, J = 7.1 Hz, phenyl of C^N^C), 7.31 (m, 4H, phenyl of C^N^C), 7.81 (d, 2H, J = 7.1 Hz, phenyl of C^N^C), 7.90 (d, 2H, J = 8.1 Hz, pyridyl of C^N^C), 8.15 (t, 1H, J = 8.1 Hz, pyridyl of C^N^C), 8.36 (s, 2H, imidazolyl of NHC). Positive FAB-MS: m/z 731 $[M - PF_6]^+$. Elemental analyses calcd for $C_{38}H_{35}N_3PF_6Au \cdot 1/2H_2O$ (found): C, 51.59 (51.46); H, 4.10 (4.23); N, 4.75 (4.74).

[Au(C^N^C)(SIMes)]PF_6 5. (SIMes = 1,3-dimesityl-4,5-dihydroimidazol-2-ylidene) Synthesized according to a procedure similar to that of **1** except 1,3-bis(2,4,6-trimethylphenyl)imidazolinium chloride (111 mg, 0.324 mmol) was used in place of 1,3-dimethylimidazolium iodide. Yellow crystals of **5** were obtained. Yield: 92 mg (42%). ^{1}H NMR (300 MHz, DMSO-d_6, 298 K): δ 2.09 (s, 6H, $-CH_3$), 2.43 (s, 12H, $-CH_3$), 4.50 (s, 4H, $-CH_2-$ in NHC), 6.84 (s, 4H,-C_6H_2-), 7.31 (t, 2H, J = 7.2 Hz, phenyl of C^N^C), 7.40 (t, 2H, J = 7.2 Hz, phenyl of C^N^C), 7.73 (d, 2H, J = 7.2 Hz, phenyl of C^N^C), 7.79 (d, 2H, J = 7.2 Hz, phenyl of C^N^C), 7.88 (d, 2H, J = 8.1 Hz, pyridyl of C^N^C), 8.13 (t, 1H, J = 8.1 Hz, pyridyl of C^N^C). Positive FAB-MS: m/z 733 $[M - PF_6]^+$. Elemental analyses calcd for $C_{38}H_{37}N_3PF_6Au \cdot CH_2Cl_2$ (found): C, 48.66 (48.53); H, 4.08 (4.08); N, 4.37 (4.54).

[Au_2(C^N^C)$_2$(MeIC$_2$IMe)](PF_6)$_2$ 6. (MeIC$_2$IMe = 1,2-bis(3-methylimidazolium-1-yl)ethane) Synthesized according to a procedure similar to that of **1**. A mixture of 1,2-bis(3-methylimidazolium-1-yl)ethane chloride (53 mg, 0.201 mmol) and potassium *tert*-butoxide (38 mg, 0.336 mmol) in methanol (60 mL) was heated to reflux for 30 min, after which [Au(C^N^C)Cl] (200 mg, 0.433 mmol) was added to give a pale yellow suspension. The resulting mixture was heated to reflux for 12 h. After cooling to room temperature, the reaction mixture was concentrated, and subjected to a metathesis reaction with ammonium hexafluorophosphate in methanol to give a yellow solid. The crude product was collected by filtration and washed with diethyl ether. Subsequent recrystallization from slow diffusion of diethyl ether vapor into the concentrated dichloromethane solution gave the titled complex as yellow crystals. Yield: 255 mg (95%). ^{1}H NMR (300 MHz, DMSO-d_6, 298 K): δ 3.66 (s, 6H, $-CH_3$), 4.65 (s, 4H, $-CH_2-$), 6.65 (d, 4H, J = 7.5 Hz, phenyl of C^N^C), 6.95 (t, 4H, J = 7.5 Hz, phenyl of C^N^C), 7.13 (t, 4H, J = 7.5 Hz, phenyl of C^N^C), 7.62 (d, 4H, J = 7.5 Hz, phenyl of C^N^C), 7.79 (d, 2H, J = 1.2 Hz, imidazolyl of NHC), 7.85 (d, 4H, J = 7.8 Hz, pyridyl of C^N^C), 7.99 (d, 2H, J = 1.2 Hz, imidazolyl of NHC), 8.19 (t, 2H, J = 7.8 Hz, pyridyl of C^N^C). Positive FAB-MS: m/z 1188 $[M - PF_6]^+$, 1043 $[M - 2PF_6]^+$. Elemental analyses calcd for $C_{44}H_{36}N_6P_2F_{12}Au_2 \cdot 2H_2O$ (found): C, 38.61 (38.39); H, 2.95 (2.84); N, 6.14 (6.54).

[Au_2(C^N^C)$_2$(MeIC$_4$IMe)](PF_6)$_2$ 7. (MeIC$_4$IMe = 1,4-bis(3-methylimidazolium-1-yl)butane) Synthesized according to a procedure similar to that of **6** except 1,4-bis(3-methylimidazolium-1-yl)butane chloride (58.5 mg, 0.201 mmol) was used in place of 1,2-bis(3-methylimidazolium-1-yl)ethane chloride. Yellow crystals of **7** were obtained. Yield: 193 mg (71%). ^{1}H NMR (400 MHz, DMSO-d_6, 298 K): δ 1.63 (s, 4H, $-CH_2-$), 3.71 (s, 6H, $-CH_3$), 4.04 (s, 4H, $-CH_2-$), 6.73 (d, 4H, J = 7.2 Hz, phenyl of C^N^C), 7.13 (t, 4H, J = 7.2 Hz, phenyl of C^N^C), 7.23 (t, 4H, J = 7.2 Hz, phenyl of C^N^C), 7.72 (s, 4H, imidazolyl of NHC), 7.82 (d, 4H, J = 7.2 Hz, phenyl of C^N^C), 7.99 (d, 4H, J = 8.0 Hz, pyridyl of C^N^C), 8.26 (t, 2H, J = 8.0 Hz, pyridyl of C^N^C). Positive FAB-MS: m/z 1215 $[M - PF_6]^+$, 1070 $[M - 2PF_6]^+$. Elemental analyses calcd for $C_{46}H_{40}N_6P_2F_{12}Au_2 \cdot 1/2CH_2Cl_2$ (found): C, 39.80 (39.79); H, 2.95 (2.98); N, 5.99 (6.23).

[Au_2(C^N^C)$_2$(MeIC$_6$IMe)](PF_6)$_2$ 8. (MeIC$_6$IMe = 1,6-bis(3-methylimidazolium-1-yl)hexane) Synthesized according to a procedure similar to that of **6** except 1,6-bis(3-methylimidazolium-1-yl)hexane chloride (64 mg, 0.200 mmol) was used in place of 1,2-bis(3-methylimidazolium-1-yl)ethane chloride. Yellow crystals of **8** were obtained. Yield: 86 mg (31%). ^{1}H NMR (400 MHz, DMSO-d_6, 298 K): δ 0.96 (s, 4H, $-CH_2-$), 1.50 (s, 4H, $-CH_2-$), 3.79 (s, 6H, $-CH_3$), 4.19 (s, 4H, $-CH_2-$), 6.80 (d, 4H, J = 7.4 Hz, phenyl of C^N^C), 7.23 (t, 4H, J = 7.4 Hz, phenyl of C^N^C), 7.33 (t, 4H, J = 7.4 Hz, phenyl of C^N^C), 7.75 (d, 4H, J = 1.8 Hz, imidazolyl of NHC), 7.83 (d, 4H, J = 1.8 Hz, imidazolyl of NHC), 7.93 (d, 4H, J = 7.4 Hz, phenyl of C^N^C), 8.00 (d, 4H, J = 8.0 Hz, pyridyl of C^N^C), 8.25 (t, 2H, J = 8.0 Hz, pyridyl of C^N^C). Positive FAB-MS: m/z 1243 $[M - PF_6]^+$, 1098 $[M - 2PF_6]^+$. Elemental analyses calcd for $C_{48}H_{44}N_6P_2F_{12}Au_2 \cdot 1/2H_2O$ (found): C, 41.25 (41.01); H, 3.24 (3.18); N, 6.01 (6.32).

[Au_2(^{t}BuC^N^C^{t}Bu)$_2$(MeIC$_2$IMe)](PF_6)$_2$ 9. (MeIC$_2$IMe = 1,2-bis(3-methylimidazolium-1-yl)ethane) Synthesized according to a procedure similar to that of **6** except [Au(^{t}BuC^N^C^{t}Bu)Cl] (248 mg, 0.433 mmol) was used in place of [Au(C^N^C)Cl]. Yellow crystals of **9** were obtained. Yield: 40 mg (13%). ^{1}H NMR (300 MHz, DMSO-d_6, 298 K): δ 0.92 (s, 36H, ^{t}Bu), 3.70 (s, 6H, $-CH_3$), 4.69 (s, 4H, $-CH_2-$), 6.61 (s, 4H, phenyl of C^N^C), 7.05 (d, 4H, J = 8.1 Hz, phenyl of C^N^C), 7.42 (d, 4H, J = 8.1 Hz, phenyl of C^N^C), 7.83 (d, 4H, J = 8.1 Hz, phenyl and pyridyl of C^N^C),

7.92 (d, 2H, $J = 1.7$ Hz, imidazolyl of NHC), 8.11 (d, 2H, $J = 1.7$ Hz, imidazolyl of NHC), 8.23 (t, 2H, $J = 8.1$ Hz, pyridyl of C^N^C). Positive FAB-MS: m/z 1268 $[M - PF_6]^+$, 1413 $[M - 2PF_6]^+$. Elemental analyses calcd for $C_{60}H_{68}N_6P_2F_{12}Au_2 \cdot 1/2CH_2Cl_2$ (found): C, 45.43 (45.49); H, 4.35 (4.41); N, 5.25 (4.90).

[Au$_2$(^{t}BuC^N^C^{t}Bu)$_2$(MeIC$_4$IMe)](PF$_6$)$_2$ 10. (MeIC$_4$IMe = 1,4-bis(3-methylimidazolium-1-yl)butane) Synthesized according to a procedure similar to that of **7** except [Au(^{t}BuC^N^C^{t}Bu)Cl] (248 mg, 0.433 mmol) was used in place of [Au(C^N^C)Cl]. Yellow crystals of **10** were obtained. Yield: 163 mg (52%). ^{1}H NMR (400 MHz, DMSO-d_6, 298 K): δ 0.95 (s, 36H, ^{t}Bu), 1.55 (s, 4H, $-CH_2-$), 3.68 (s, 6H, $-CH_3$), 4.02 (s, 4H, $-CH_2-$), 6.68 (s, 4H, phenyl of C^N^C), 7.04 (d, 4H, $J = 8.1$ Hz, phenyl of C^N^C), 7.44 (d, 4H, $J = 8.1$ Hz, phenyl of C^N^C), 7.83 (d, 2H, $J = 1.8$ Hz, imidazolyl of NHC), 7.88 (d, 2H, $J = 1.8$ Hz, imidazolyl of NHC), 7.90 (d, 4H, $J = 8.1$ Hz, phenyl and pyridyl of C^N^C), 8.29 (t, 2H, $J = 8.1$ Hz, pyridyl of C^N^C). Positive FAB-MS: m/z 1296 $[M - PF_6]^+$, 1441 $[M - 2PF_6]^+$. Elemental analyses calcd for $C_{62}H_{72}N_6P_2F_{12}Au_2 \cdot 1/2CH_2Cl_2$ (found): C, 46.12 (45.86); H, 4.52 (4.55); N, 5.16 (5.34).

[Au$_2$(^{t}BuC^N^C^{t}Bu)$_2$(MeICBClIMe)](PF$_6$)$_2$ 11. (MeICBClIMe = 2,6-bis(1-methylimidazolium-3-yl)pyridine) Synthesized according to a procedure similar to that of **6** except 2,6-bis(1-methylimidazolium-3-yl)pyridine dibromide (86 mg, 0.201 mmol) was used in place of 1,2-bis(3-methylimidazolium-1-yl)ethane chloride. Yellow crystals of **11** were obtained. Yield: 161 mg (57%). ^{1}H NMR (400 MHz, DMSO-d_6, 298 K): δ 3.76 (s, 6H, $-CH_3$), 4.97 (s, 4H, $-CH_2-$), 6.71 (d, 2H, -Ar), 6.94 (s, 2H, imidazolyl of NHC), 7.17 (t, 2H, $J = 7.4$ Hz, phenyl of C^N^C), 7.29 (t, 2H, $J = 7.4$ Hz, phenyl of C^N^C), 7.66 (d, 1H, $J = 2.0$ Hz, -Ar), 7.79 (d, 1H, $J = 2.0$ Hz, -Ar), 7.87 (d, 2H, $J = 7.4$ Hz, phenyl of C^N^C), 7.93 (d, 2H, $J = 8.0$ Hz, pyridyl of C^N^C), 8.18 (t, 1H, $J = 8.0$ Hz, pyridyl of C^N^C). Positive FAB-MS: m/z 1265 $[M - PF_6]^+$, 1120 $[M - 2PF_6]^+$. Elemental analyses calcd for $C_{50}H_{40}N_6P_2F_{12}Au_2 \cdot CH_2Cl_2$ (found): C, 41.01 (41.05); H, 2.83 (2.89); N, 5.63 (5.94).

Acknowledgment. V.W.-W.Y. acknowledges support from The University of Hong Kong under the Distinguished Research Achievement Award Scheme, the World Gold Council GROW Programme, and the URC Strategic Research Theme on Molecular Materials. This work has been supported by a GRF grant from the Research Grants Council of Hong Kong Special Administrative Region, China (HKU 7057/07P). V.K.-M.A. acknowledges the receipt of a postgraduate studentship from The University of Hong Kong.

Supporting Information Available: Perspective drawings of **2**, **5**, **7**, **9**, and **10**; crystal packing diagrams of **1**, **2**, **5**, **7**, and **9**−**11**; and crystallographic data for **1**−**3**, **5**−**7**, and **9**−**11**. This material is available free of charge via the Internet at http://pubs.acs.org.

JA9027692